(Received 8 March 2025, Accepted 11 May 2025, Scheduled 25 May 2025)

Numerical Analysis of Electric Field Distribution in Segmented Lightning Diverter Strip

Rudra Narayan Barik and Hrishikesh Shashikant Sonalikar*

Department of Electrical & Electronics Engineering, BITS Pilani, Goa Campus, India

ABSTRACT: This paper investigates the distribution of the electric field around a circular segmented diverter strip designed for lightning protection. This is accomplished by performing parametric analysis on various geometry parameters of the circular-shaped segmented lightning diverter strip and numerically calculating the electric field and crossover voltage using full-wave simulation. The results demonstrate that as the spacing between the segments decreases, there is a significant increase in electric field strength, reaching a maximum value of 438.22 MV m^{-1}, while the crossover voltage decreases from 2990.59 V to 744.35 V. An increase in the diameter of the segments is associated with a stronger electric field, with the maximum field strength reaching 300.36 MV m^{-1}, while in this case, the crossover voltage decreases from 1493.36 V to 1462.36 V. In contrast, the electric field increases as the segment height decreases, with no significant change in the crossover voltage. The study also analyzes the impact of curvature and different substrate materials on the electric field distribution and crossover voltage. Additionally, simulation results on the electric field distribution and capacitance calculations for various segments of the diverter are utilized to predict the probable location of the lightning attachment.

1. INTRODUCTION

A Lightning Protection System (LPS) is designed to protect airplanes, rotorcraft, and wind turbines from the damaging effects of lightning strikes by safely directing electrical energy to the ground [1, 2]. Before the development of modern LPS, metallic skins were used in aircraft, and metallic rods were utilized for wind turbines to offer protection against lightning strikes [3, 4]. However, the heavy weight of these structures rendered them unsuitable for protecting aircraft and wind turbines from lightning strikes. Also, they significantly attenuated the electromagnetic signals when being used around the communication systems of an airplane [5]. These structures are also prone to corrosion and temperature sensitivity. Subsequent advancements in materials technology enabled the use of metallic layers, sprays, and metal-coated fibers for protection against lightning [6, 7]. Recent advances in identifying specific areas of aircraft and wind turbines that are vulnerable to lightning strikes have enabled engineers to design lightning diverters strategically placed in these locations to provide effective protection from lightning strikes [8, 9].

Lightning diverters are metallic strips designed to safely redirect high-voltage lightning currents away from critical components of aircraft and wind turbines by providing a low resistance, controlled pathway toward the ground [10]. Generally, two types of lightning diverters are used in LPS: solid and segmented. Solid diverters are continuous metal strips providing an uninterrupted path to discharge lightning current to the ground [11]. In contrast, the segmented diverters comprise a series of metal segments placed on an insulating material. During lightning strikes, the intense electric field (E-field) ionizes the air gaps between the metal segments. This ionization forms a plasma channel above the air gaps, providing a low-resistance path for the lightning current, which is then safely directed to the ground [12]. Segmented diverters are commonly utilized in wind turbines due to their lightweight design and ease of mounting on the turbine blades [13]. Segmented diverters are also preferred for protecting aircraft radomes from lightning due to their minimal impact on antenna radiation pattern [14].

The research on segmented diverters for lightning protection systems has evolved through critical research contributions. Ref. [15] presents the optimization of the length and number of diverters required to shield the radome-enclosed antenna from lightning discharge. Similarly, the optimization of the layout of the diverter strips for aircraft radomes is documented in [16]. This article shows that segmented diverters have less influence on antenna gain (< 0.5 dB) than solid diverters (4.5 dB). Subsequently, the impact of the spacing between the metallic segments of the diverter strip on antenna radiation patterns is analyzed in [17] and [18]. It is demonstrated that diverter strips with increased separation between segments lead to less significant interference with the antenna's near-field. The article in [5] contributes to the design and testing of a full-scale SATCOM radome prototype with an optimized arrangement of solid and segmented diverter strips for lightning protection. The research in [19] and [20] further predicts that larger metallic segments with smaller air gaps are preferable for LPS. Additionally, it was established that the conductive properties of the panel to which the segmented strip is attached can reduce the peak E-field in the gaps. From these works, it can be observed that the design and analysis of the lightning protection system involves

* Corresponding author: Hrishikesh Shashikant Sonalikar (hrishikeshs@goa.bits-pilani.ac.in).

both simulation and experimental validation. Although experimental studies, such as those reported in [21] and [22], are required before the deployment of LPS, they are often expensive and time-consuming. In contrast, simulation-based studies provide a low-cost, versatile design approach for visualizing complex 3-D field interactions that are hard to replicate experimentally [23, 24].

The protection against lightning strikes offered by segmented diverters depends upon the distribution of the E-field around the segments. Also, understanding the E-field dynamics is crucial for optimizing the geometrical design of these diverters to enhance their lightning protection capabilities. In the literature, only a few works present a detailed parametric study of the segmented diverters showing the E-field distribution.

This article offers insights into the E-field distribution around a circular segmented diverter strip for lightning protection. Section 2 describes the modeling of the diverter geometry. The influence of different geometrical parameters, such as diameter, spacing, and height of the metal segments, on the distribution of the E-field and crossover voltage is analyzed in Section 3. Also, the probable location of lightning attachment is identified using electrostatic simulations and computation of the capacitance of different segments of the diverter. Finally, Section 5 concludes the paper with remarks.

2. MODELING OF SEGMENTED DIVERTER STRIP

The diverter strip consists of circular metallic segments placed over a planar dielectric slab, as shown in Fig. 1. The segments typically have shapes such as circle, square, oval, or diamond. A circular shape is used in this work as it is very common in segmented diverters [25]. The inset of the figure illustrates the height (H), diameter (D) of each segment, and spacing (S) between the segments. The material used for segments is Aluminum [16, 26], having electrical conductivity of $3.56 \times 10^7\,\mathrm{Sm}^{-1}$. Pyroceram 9606 ($\epsilon_r = 5.515$ and $\tan\delta = 0.0003$, measured at room temperature) is used as the dielectric substrate. Pyroceram 9606 is selected for its ability to withstand high E-field during a lightning strike without breaking down.

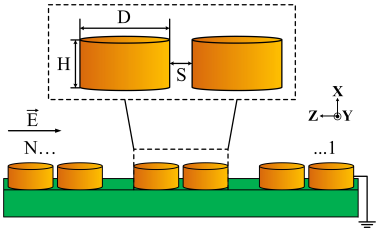

FIGURE 1. Diverter strip with circular segments placed in an ambient E-field. The inset illustrates the geometry parameters used in the parametric study.

To study the distribution of the E-field on the diverter strip geometry, it is placed in a rectangular simulation volume. Two opposite surfaces of the simulation volume are plates of perfect electric conductors (PECs) used to generate an ambient E-field directed along the negative Z-direction, as shown in Fig. 1. Segment 1 is connected to the ground plate. To eliminate fringing fields, PMC (perfect magnetic conductor) boundary conditions are applied to the four remaining surfaces of the simulation volume. The dimensions of the dielectric substrate are thickness $(x) = 2\,\mathrm{mm}$, length $(z) = 209\,\mathrm{mm}$, and width $(y) = 5\,\mathrm{mm}$. The diameter (D) and height (H) of the segments are 5 mm and 2 mm, respectively, with a spacing (S) of 0.5 mm between them. The diverter strip consists of $N = 30$ segments placed on the dielectric substrate.

The PEC plates are excited with the standard voltage waveform B as shown in Fig. 2 [27], as it best represents the E-field associated with lightning reattachment to the object under test [28]. T_1 represents the time to rise from 10% to 90% of the crest (V_{peak}), and T_2 represents the time to decay to half the crest ($V_{50\%}$) amplitude. The standard analytical expression of the B-waveform is [29]

$$V = 1050\left[e^{-(t/70\,\mu s)} - e^{-(t/0.4\,\mu s)}\right]\ \mathrm{kV}. \tag{1}$$

The peak value of the electric potential achieved using this waveform is 1 MV.

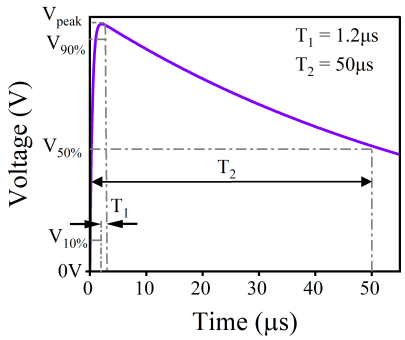

FIGURE 2. Standard voltage waveform B to represent the E-field associated with a lightning strike.

The LF-TDS (Low-Frequency Time Domain Solver) of the CST MWS (Computer Simulation Technology Microwave Studio) [30] is used to analyze the system by computing the potential difference and the E-field distribution around the segments of the diverter strip.

3. RESULTS

Although air is generally a good insulator, it may become partially conductive when being exposed to a strong E-field. The dielectric strength of dry air at standard temperature and pressure (STP) is $3\,\mathrm{MV\ m}^{-1}$. When the ambient E-field crosses this threshold, the air breaks down and becomes conductive, thus creating a channel for lightning [31]. The crossover voltage, $V_{crossover}$ (V), is the difference in potential between two consecutive segments when the E-field crosses this threshold value [32].

The results presented in this section are evaluated at the peak of the B-waveform, which occurs at 2.1 µs, representing the point at which the E-field reaches its maximum value. Numerical results are presented at the midpoint of gaps no. 1, 15, and 29, which are located at the start, middle, and end of the diverter strip, respectively. Graphical results of E-field distribution are presented for gap no. 15 as an example.

TABLE 1. Magnitude of E-field components at different gap positions.

Gap No.	$\lvert E_x\rvert$	$\lvert E_y\rvert$	$\lvert E_z\rvert$
	(MV m^{-1})		
1	6.13	15.60	206.06
15	4.74	0.78	44.72
29	2.27	0.02	30.11

TABLE 2. $\lvert E\rvert$ and $V_{crossover}$ for different spacings, S.

Spacing (S)	$\lvert E\rvert$ (MV m^{-1}) at gap no.			$V_{crossover}$ (V)
(mm)	1	15	29	at gap no. 15
0.25	438.22	88.64	54.67	744.35
0.50	206.54	44.97	30.19	1491.23
1.00	93.15	24.27	17.64	2990.59

To obtain the initial idea about the E-field and potential distribution in the vicinity of segmented diverters, the electric potential is calculated along the straight line curves at two positions as shown in Fig. 3. Both the curves start at the grounded segment 1 and end at the last segment 30 of the diverter strip. At Pos. 1, the curve encounters the top flat surface of the circular segments. Pos. 2 is 2 mm above the surfaces of the segments. It can be observed that the potential increases as the field point is moved from segment 1 to segment 30 at Pos. 2. Also, the potential at Pos. 1 shows steps due to the equipotential surfaces of the circular segments. Potential increases in the gap between the segments at Pos. 1. The insets in the figure show the electric potential calculated at gaps 1 and 29 of the segmented diverter. The corresponding E-field is determined to be 206.06 MV m^{-1} at gap 1 and 30.11 MV m^{-1} at gap 29.

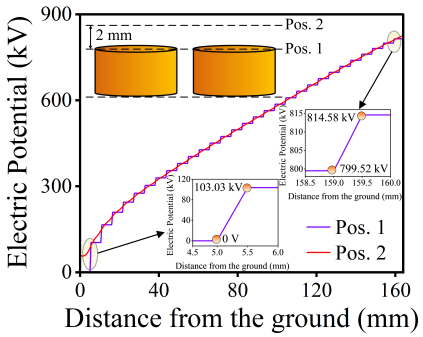

FIGURE 3. Electric potential (kV) over the segmented diverter strip with distance from the ground (mm) for segments having diameter $D = 5$ mm, height $H = 2$ mm, and spacing $S = 0.5$ mm. Pos. 1 indicates the variation of potential along the surface of the segments, while Pos. 2 shows its variation 2 mm above the surface.

The components of the E-field vector are calculated at the mid-points of different gap positions of the diverter strip and tabulated in Table 1. It can be observed that the magnitude of the Z-component of the E-field is significantly higher than that of the X- and Y-components at each gap position.

Figure 4 shows the E-field distribution across the gap between the segments of the diverter strip as the spacing between the segments is changed from 0.25 mm to 1 mm while maintaining $D = 5$ mm and $H = 2$ mm. It can be seen that the strength of the E-field is inversely proportional to the spacing between the segments. The same observation can be made from the values of E-field presented in Table 2. $|E|$ is the magnitude of the total E-field computed at each of the gap centers. The crossover voltage is presented only for Gap-15 since its value is the same in different gaps. The E-field becomes weak as the spacing between the segments is increased from 0.25 mm to 1 mm across all gap positions. Also, it is observed that the E-field strength is higher at gap-1 (near the ground plane) and lower as the point of observation moves toward gaps 15 and 29. The crossover voltage increases with an increase in spacing between the segments.

Figure 5 shows the E-field distribution across the gaps for different diameters of the circular segments. The diameter is changed from 4 mm to 6 mm while maintaining $S = 0.5$ mm and $H = 2$ mm. It can be seen that the strength of the E-field is directly proportional to the diameter of the segments. This is further supported by the data shown in Table 3. It can be seen that the E-field becomes stronger as the diameter of the segments is increased across all gap positions. The crossover voltage shows a reduction as the diameter is increased.

It is evident from the above observations that larger segments with less spacing contribute to a stronger E-field. When the spacing between segments is reduced, the E-field becomes stronger because minimizing the distance between the conducting surfaces concentrates the potential difference over a smaller area. As the diameter of the segments increases, the total charge that each segment can store also increases since the surface area expands with the square of the radius. A larger conductor typically produces a stronger E-field at its surface due to the increased total charge [15, 19].

Figure 6 shows the E-field distribution across the gap as the height of the segments is changed from 2 mm to 0.5 mm while maintaining $S = 0.5$ mm and $D = 5$ mm. The graphical results do not indicate a significant change in the E-field with variations in the segment height. However, the data presented in Table 4 indicate that the E-field increases with a decrease in the height of the segments. Also, the height of the segment does not have a significant impact on the crossover voltage.

The other parameter that affects the geometry of the diverter strip is the curvature. Until now, the computations were performed on a planar diverter strip. In reality, however, in applications such as a streamlined radome placed over an airborne antenna, the diverters are attached to a curved substrate. In this context, the curvature of the diverter for a typical tangent-ogive radome is considered. The standard equation for determining the radius of curvature R for a tangent-ogive radome is:

$$R = \frac{D^2 + 4L^2}{4D}, \tag{2}$$

where L and D represent the length and diameter of the tangent-ogive radome, respectively. For a typical radome with a length of $L = 250$ mm and a diameter of $D = 125$ mm, the radius R is 531.25 mm. Fig. 7 illustrates the distribution of the E-field across gap-15 for different curvatures of the diverter strip.

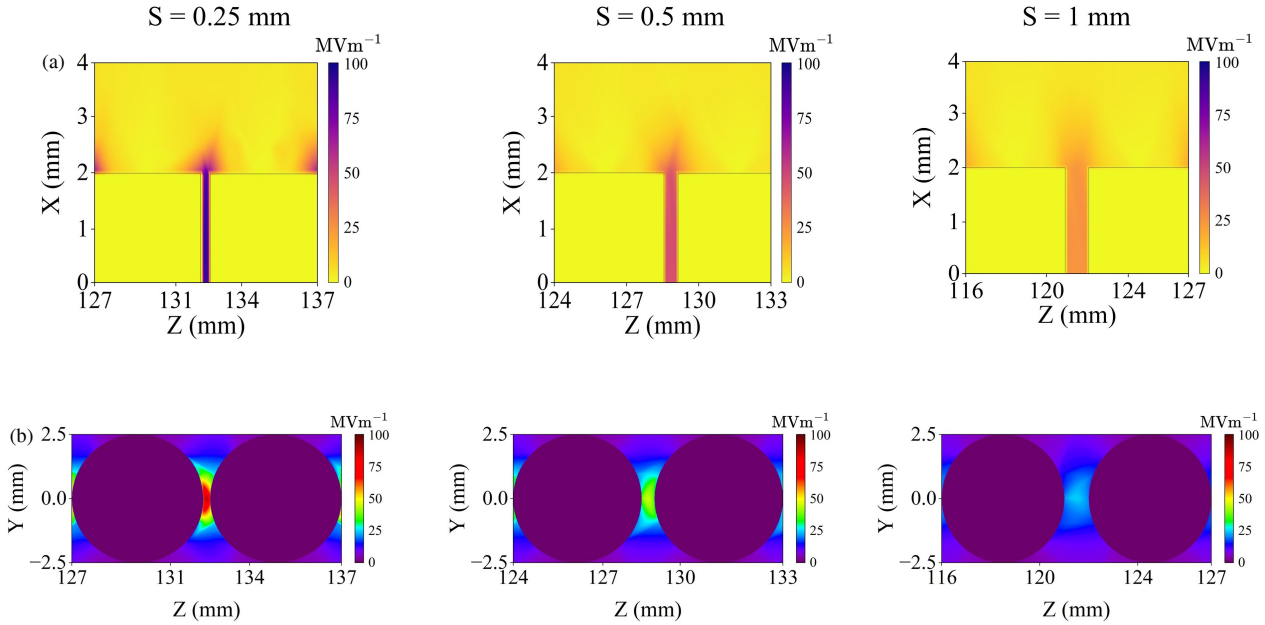

FIGURE 4. Distribution of the E-field around gap-15 for different segment spacings, S: (a) side view and (b) top view.

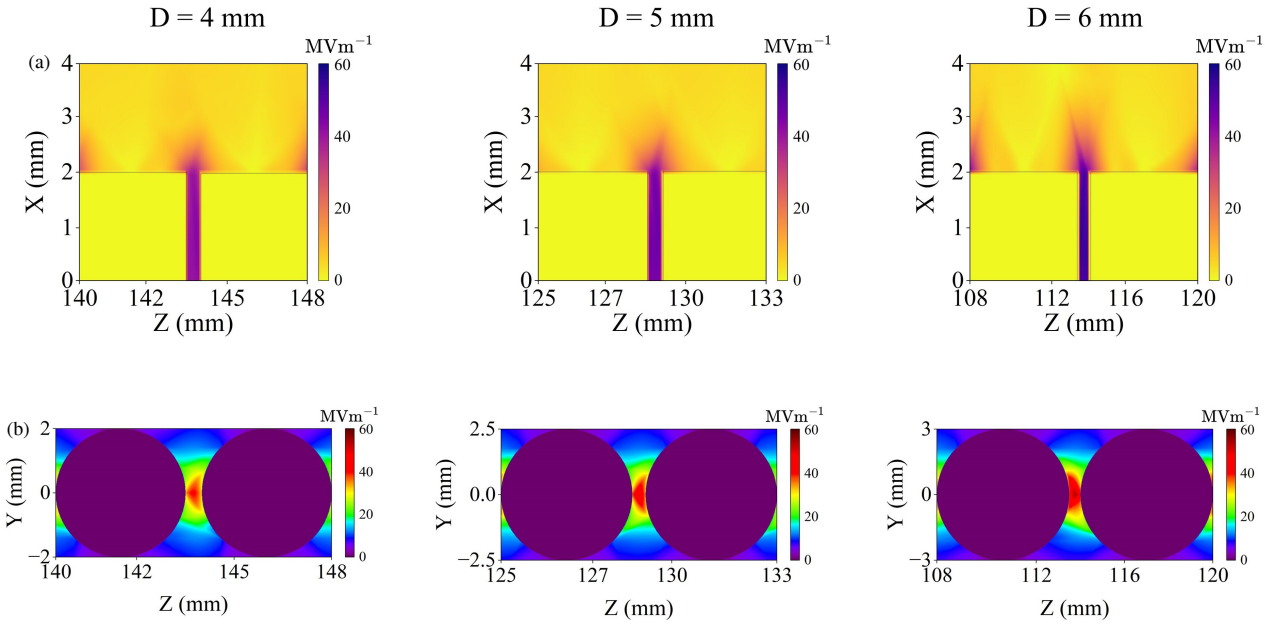

FIGURE 5. Distribution of the E-field around gap-15 for different segment diameters, D: (a) side view and (b) top view.

TABLE 3. $|E|$ and $V_{crossover}$ for different diameters, D.

Diameter (D) (mm)	$\|E\|$ (MV m^{-1}) at gap no. 1	15	29	$V_{crossover}$ (V) at gap no. 15
4	126.09	40.34	26.56	1493.36
5	206.54	44.97	30.19	1491.23
6	300.36	53.41	36.28	1462.36

TABLE 4. $|E|$ and $V_{crossover}$ for different heights, H.

Height (H) (mm)	$\|E\|$ (MV m^{-1}) at gap no. 1	15	29	$V_{crossover}$ (V) at gap no. 15
2.0	206.54	44.86	30.19	1491.23
1.0	220.17	44.97	30.88	1484.58
0.5	226.43	46.12	31.07	1491.21

Here, R, $0.5R$, and $0.2R$ represent the increasing degrees of curvature of the diverter strip. Specifically, as the value decreases from R to $0.2R$, it indicates an increase in curvature (bending) of the strip. Graphical results show that as curvature increases, there is no significant change in the E-field distribution. However, Table 5 shows that there is a reduction in $|E|$

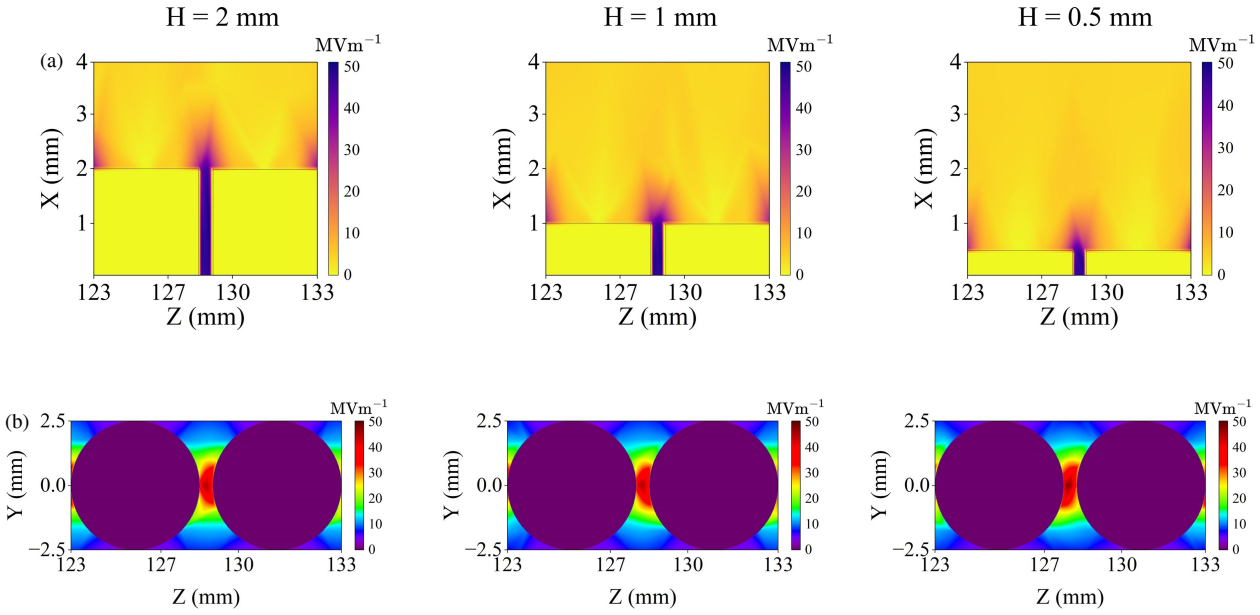

FIGURE 6. Distribution of the E-field around gap-15 for different segment heights, H: (a) side view and (b) top view.

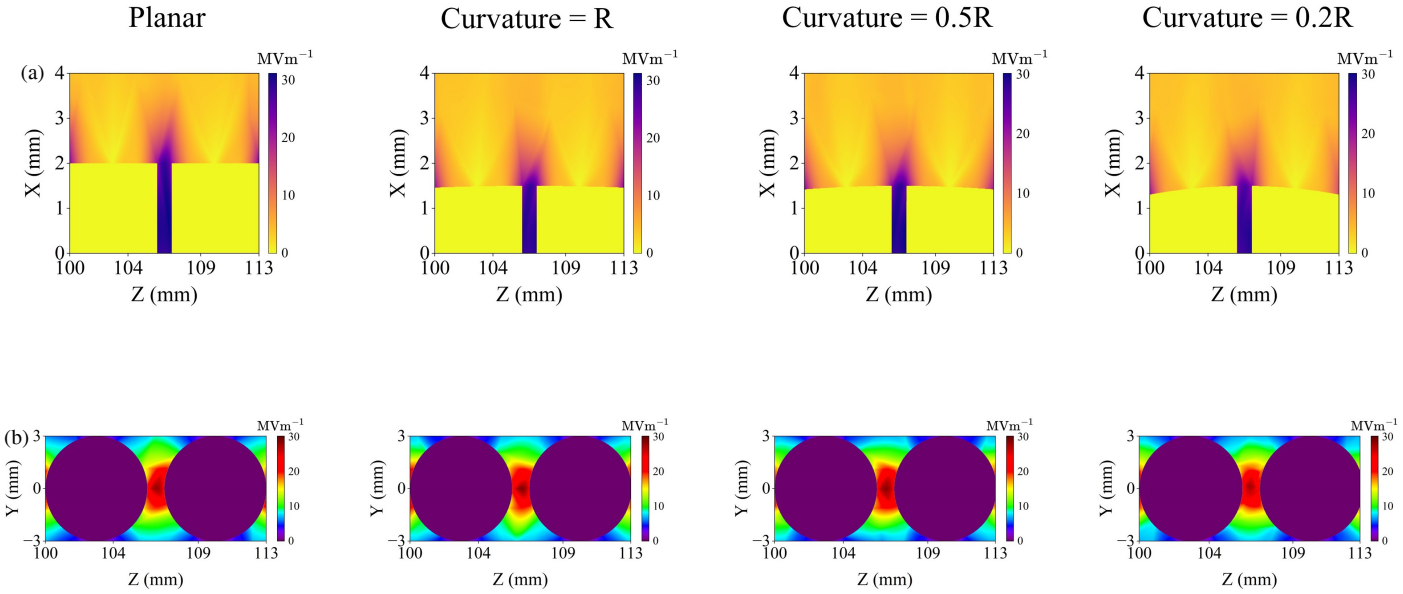

FIGURE 7. Distribution of the E-field around gap-15 for different curvatures of the diverter strip: (a) side view and (b) top view.

TABLE 5. $|E|$ and $V_{crossover}$ at Gap-15 for different curvatures.

Curvature	$\|E\|$ (MV m^{-1})	$V_{crossover}$ (V)
Planar	28.43	2959.19
R	28.39	2960.09
$0.5R$	27.99	2986.77
$0.2R$	25.95	3108.97

TABLE 6. $|E|$ and $V_{crossover}$ at Gap-15 for different substrate materials.

Substrate Material	ϵ_r	$\tan\delta$	$\|E\|$ (MV m^{-1})	$V_{crossover}$ (V)
Pyroceram 9606	5.5	0.0003	28.01	2887.62
Fused Silica	3.8	0.0020	28.27	2985.92
Duroid	2.2	0.0009	28.36	2985.87
Teflon	2.1	0.0002	28.35	2985.86

from 28.43 MV m^{-1} to 25.95 MV m^{-1} when the curvature of the substrate increases. Increased curvature also results in an increase in the crossover voltage of the gaps from 2959.19 V to 3108.97 V.

Different applications may use different dielectric materials for the installation of segmented diverters for lightning protection. Therefore, the effect of different dielectric material properties is analyzed and shown in Table 6. It can be observed that

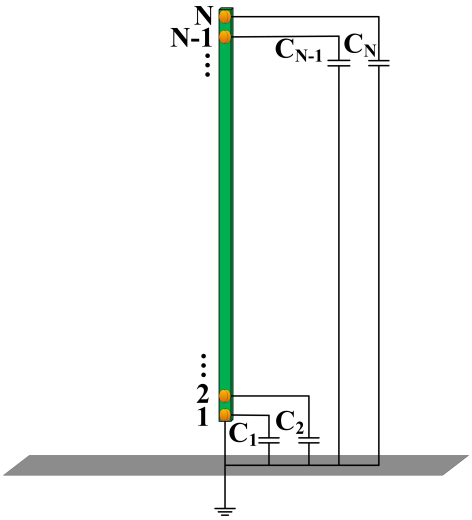

FIGURE 8. Setup for computation of capacitance for different segments to determine the segment with the least time constant for lightning conduction.

the E-field strength increases as the value of ϵ_r decreases, with the crossover voltage remaining nearly constant.

The capacitance between the segments of a diverter strip and the ground is a key factor in identifying the probable initial point of lightning attachment. In [32], the mechanism of lightning flashover of a segmented diverter strip attached to the surface of an aircraft radome is described using an equivalent RC circuit. In this model, each conductive segment of the strip is treated as having its own capacitance (C) relative to the ground, while the underlying dielectric substrate functions as a resistor (R). It has been established that the segment with the lowest capacitance will exhibit the shortest RC time constant, allowing it to respond more rapidly to external electric fields. Consequently, this segment becomes the most probable initial point of lightning attachment.

Figure 8 shows the simulation setup used to verify the aforementioned theory. In this setup, the diverter strip consists of N conductive segments, with each segment forming some capacitance with the ground. These are denoted as C_1, C_2, C_3 ... C_N, respectively. The capacitance (C) of each segment can be obtained by applying a voltage (V) of 1 V to the segment of interest and numerically computing the total charge (Q) present on the segment (using the relation $Q = CV$). The geometry parameters of the diverters used in this computation are diameter $(D) = 5$ mm, height $(H) = 2$ mm, and spacing $(S) = 0.5$ mm.

Table 7 presents the computed capacitance values for three representative segments: Segments 1, 15, and 30. Since segment 1 is closest to the ground, it shows a higher value of 10.06 pF than the capacitance values of segments 15 and 30. In

TABLE 7. Capacitance between different segments and the ground plane.

Segment No.	Capacitance (pF)
1	10.06
15	0.43
30	0.37

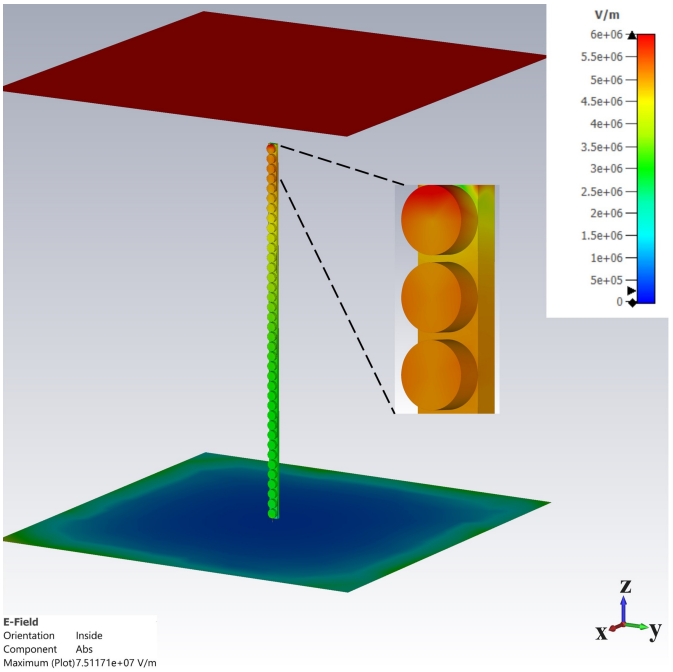

FIGURE 9. Simulation result showing the possible lightning attachment point. The segment with the maximum E-field distribution corresponds to the primary point of lightning attachment.

contrast, Segment 30 exhibits the lowest capacitance of 0.37 pF, which implies a shorter RC time. This suggests that segment 30 is the most probable point for the initial attachment of lightning.

This is further verified by calculating the E-field using the electrostatic (E-static) solver of CST MWS. The simulation results obtained are shown in Fig. 9. The simulation uses the same setup described in Section 2. The figure shows the E-field distribution when a constant potential difference of 1 MV is applied between the PEC plates. It can be observed that the E-field is maximum for the segment closer to the top PEC plate, and it gradually decreases towards the grounded PEC plate. Thus, the segment closer to the ambient E-field might be the probable point of lightning attachment. Both the above observations corroborate with the results presented in [29] and [32], which demonstrated that the tri-junction — the point where the diverter, substrate, and air meet — is the primary location for lightning attachment.

4. DISCUSSION

Analysing the impact of geometrical parameters on the distribution of E-field strength is essential for optimizing the design of segmented diverters. Fig. 10 shows the variation of E-field with (a) spacing, (b) diameter, (c) height, (d) curvature, and (e) dielectric constant of the segmented diverter. It can be observed that reducing the spacing between segments increases the E-field intensity exponentially. Larger diameters cause a linear increase in field strength. Increasing the segment height results in a linear decrease in E-field strength. The increase in curvature and dielectric constant reduces E-field strength exponentially, but the reduction is relatively small.

TABLE 8. Comparison of our work with the works done in the literature.

Reference	Major Contributions	Remarks
[15]	This work combines simulation and experimental methods to analyze how the diameter, thickness, and spacing of segments affect the electric field at both the tip and base of a hemispherical radome.	The results indicate that the electric field at the base measures 517 MV m^{-1}, which is higher than the 477 MV m^{-1} recorded at the tip.
[17]	This simulation work examines how segmented diverter strips, varying in shape, size, and spacing between metallic segments, impact the surface electric field of an ogive radome.	The results indicate that the surface electric field increases with larger segment sizes and reduced spacing between the segments.
[19]	This simulation and experimental work investigates the effects of the size and spacing between segments of a diverter on the electric field for a planar radome.	The E-field increases with increased diameter and reduced spacing between the segments. The maximum E-field observed for a diameter of $D = 3.17$ mm was 417 MV m^{-1}, while for $D = 1.52$ mm, it was 208 MV m^{-1}. Additionally, the maximum E-field at a spacing of $S = 0.2$ mm reached 500 MV m^{-1}, compared to 250 MV m^{-1} for $S = 1$ mm.
[20]	This work presents an experimental and numerical transient 2D Multiphysics model to predict the location of lightning attachment and explores the factors affecting breakdown voltage.	The results show that the breakdown voltage increases linearly with the spacing between the segments.
[22]	This experimental work presents the design and testing of lightning protection for an aircraft radome subjected to direct lightning strikes.	The results indicate that larger segments have lower breakdown voltages, but smaller segments can better withstand high current loads.
[28]	In this experimental work, high-voltage initial leader attachment tests were conducted on a full-scale UAV SATCOM radome prototype. These tests aimed to identify the optimal locations for segmented diverters and potential lightning attachment points.	It was found that intensified electric fields are essential for igniting the segmented diverters, and there is a significant voltage drop along the ignited diverter.
[32]	This experimental work aimed to gather data on the flashover characteristics of segmented diverters to ensure optimal protection for the enclosed antenna.	It was shown that when the antenna was positioned very close to the radome wall (1.5 cm away), a minimum spacing of 30 cm between the diverters was necessary to prevent dielectric breakdown. However, when the antenna was placed further away (15 cm), the diverters could be safely spaced 60 cm apart.
Our work	The simulation work shows the effect of spacing, diameter, height, curvature, and substrate material on the E-field for a planar segmented diverter.	Numerical analysis demonstrates that segments with larger diameters and reduced spacing yield an intensified E-field. E-field strength increases as height decreases and strengthens as the dielectric constant decreases. An increase in curvature results in E-field strength reduction.

Segmented diverters are used to protect aircraft radomes and wind turbine blades from lightning strikes. In aircraft, reducing the spacing or increasing the diameter of the segments enhances the electric field in the gaps, which leads to the creation of a plasma channel for the conduction of lightning current. However, when the segments are closely spaced, it reduces the RF transparency of the radome. Therefore, choosing the optimal spacing requires a balance between lightning protection and signal transmission. Also, reduced spacing and increased diameter of segments will cause proportionate increase in the weight of the radome or wind turbine blade. Reducing the height of the segments increases the strength of the electric field in the gaps. But it will also create plasma channel close to the surface of the radome or wind turbine blade. Increased height of the segments may also affect aerodynamic properties of radome or wind turbine blade. Our results show that there is relatively small change in the E-field due to the curvature of the substrate. As a result, segmented diverters can be conveniently installed on curved surfaces of radomes and wind turbine blades. Lastly, the dielectric constant has relatively small impact on the E-field strength. Therefore, the design engineer has a fair amount of choice in the selection of the substrate material based on the type of application. These findings support tailored design strategies for effective lightning protection in both aerospace and wind energy applications.

Table 8 shows the comparison between our work with those available in the existing literature. It can be observed that our work is in good agreement with the work done in various literature related to segmented diverters. Also, our work does a comprehensive analysis on the impact of geometry parameters on the E-field and crossover voltage.

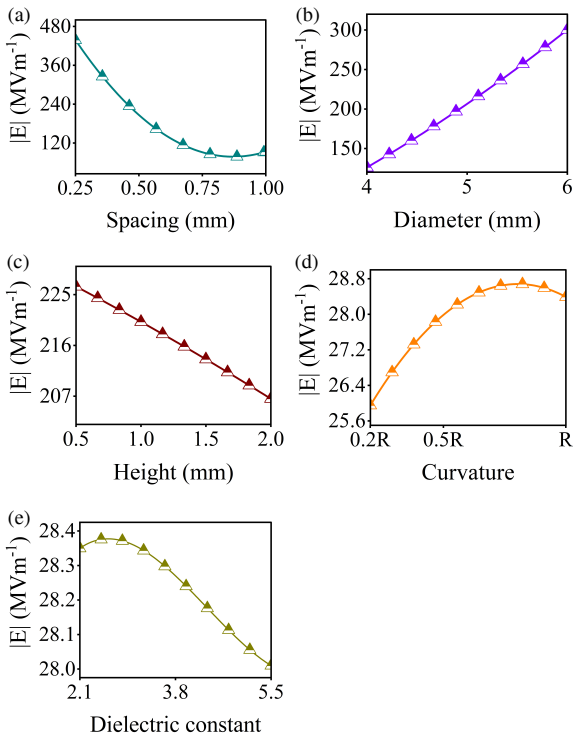

FIGURE 10. Variation of E-field with (a) spacing, (b) diameter, (c) height, (d) curvature, and (e) dielectric constant of the segmented diverter.

5. CONCLUSION

This study elucidates the influence of geometrical parameters on the E-field distribution in circular segmented diverters for LPS. It can be observed that reducing the spacing between segments increases E-field intensity exponentially. Larger diameters cause a linear increase in field strength. Increasing the segment height results in a linear decrease in E-field strength. The increase in curvature and dielectric constant reduces E-field strength exponentially, but the reduction is relatively small. The results further show that as the spacing between the segments increases, the crossover voltage also increases. However, as the diameter of the segments gets larger, the crossover voltage decreases. There is no significant change in the crossover voltage with changes in height or substrate material. The investigation into the capacitance further provides information regarding the segment having the least time constant for lightning attachment. It is estimated that the segment closer to the direction of the ambient E-field might be the primary point for lightning attachment. The E-field distribution obtained using the E-static solver of CST MWS provides further confirmation of the lightning attachment point. This research provides valuable insights into the E-field characteristics of circular segmented diverters, aiding in the improved design and optimization of diverter strips for lightning protection systems. Understanding the behavior of the E-field in segmented diverters could greatly enhance the reliability and safety of aerial and renewable energy systems in areas prone to lightning strikes. However, it is important to note that the actual behavior of lightning diverter involves complex phenomena such as plasma formation and needs experimental validation.

ACKNOWLEDGEMENT

This work was supported by the Aeronautics Research and Development Board of Defence Research and Development Organization, Government of India. We are thankful to Shri. G. V Ramakoteshwar Rao for his valuable discussions during the preparation of this manuscript.

REFERENCES

[1] Plumer, J. A. and J. D. Robb, "The direct effects of lightning on aircraft," *IEEE Transactions on Electromagnetic Compatibility*, No. 2, 158–172, 1982.

[2] Yasuda, Y., S. Yokoyama, M. Minowa, and T. Satoh, "Classification of lightning damage to wind turbine blades," *IEEJ Transactions on Electrical and Electronic Engineering*, Vol. 7, No. 6, 559–566, 2012.

[3] Ikhazuangbe, G. I., C. Gomes, S. Mohanna, B. Dagogo, O. N. Osarimwian, E. Jaja, and P. T. Alole, "A review of lightning protection methods for wind turbine blades," *IOSR Journal of Electrical and Electronics Engineering (IOSR-JEEE)*, Vol. 18, No. 1, 01–13, 2023.

[4] Fisher, F. A. and J. A. Plumer, "Lightning protection of aircraft," Tech. Rep., NASA, 1977.

[5] Karch, C., F. Heidler, and C. Paul, "Protection of aircraft radomes against direct lightning strikes — An overview," *Atmosphere*, Vol. 12, No. 9, 1141, 2021.

[6] Gagné, M. and D. Therriault, "Lightning strike protection of composites," *Progress in Aerospace Sciences*, Vol. 64, 1–16, 2014.

[7] Evans, S., I. Revel, M. Cole, and R. Mills, "Lightning strike protection of aircraft structural joints," in *2014 International Conference on Lightning Protection (ICLP)*, 1952–1959, Shanghai, China, Oct. 2014.

[8] Lalande, P. and A. Delannoy, "Numerical methods for zoning computation," *Aerospace Lab*, No. 5, p–1, 2012.

[9] Madsen, S. F., K. Bertelsen, T. H. Krogh, H. V. Erichsen, A. N. Hansen, and K. B. Lønbæk, "Proposal of new zoning concept considering lightning protection of wind turbine blades," in *2010 30th International Conference on Lightning Protection (ICLP)*, 1–7, Cagliari, Italy, Sep. 2010.

[10] Amason, M. P. and G. J. Cassell, "Radome lightning protection techniques and their electromagnetic compatibility," in *1970 IEEE Electromagnetic Compatibility Symposium Record*, 1–19, Anaheim, CA, USA, Jul. 1970.

[11] Piche, A., G.-P. Piau, C. Bernus, F. Campagna, and D. Balitrand, "Prediction by simulation of electromagnetic impact of radome on typical aircraft antenna," in *The 8th European Conference on Antennas and Propagation (EuCAP 2014)*, 3205–3208, The Hague, Netherlands, Apr. 2014.

[12] Elkalsh, A., P. Sewell, T. M. Benson, and A. Vukovic, "Coupled electrothermal two-dimensional model for lightning strike prediction and thermal modeling using the TLM method," *IEEE Journal on Multiscale and Multiphysics Computational Techniques*, Vol. 2, 38–48, 2017.

[13] Hansen, L. B., J. Korsgaard, and I. Mortensen, "Improved lightning protection system enhances the reliability of multi-MW blades," *LM Glasfiber A/S, Lunderskov, DK, www. Imglasfiber. com*, 1–11, 2005.

[14] Ayub, A. S., W. H. Siew, and S. J. MacGregor, "Lightning protection of wind turbine blades — An alternative approach," in *2011 7th Asia-Pacific International Conference on Lightning*, 941–946, Chengdu, China, Nov. 2011.

[15] Petrov, N. I., A. Haddad, G. N. Petrova, H. Griffiths, and R. T. Waters, "Study of effects of lightning strikes to an aircraft," in *Recent Advances in Aircraft Technology*, Intechopen, 2012.

[16] Yanchao, D., X. Xiu, and H. U. Pingdao, "Research on aircraft radome lightning protection based on segmented diverter strips," in *2017 International Symposium on Electromagnetic Compatibility — EMC EUROPE*, 1–6, Angers, France, Sep. 2017.

[17] Vukovic, A., P. Sewell, and T. M. Benson, "Impact of in situ radome lightning diverter strips on antenna performance," *IEEE Transactions on Antennas and Propagation*, Vol. 68, No. 11, 7287–7296, 2020.

[18] Vukovic, A., P. Sewell, T. M. Benson, C. C. R. Jones, and S. Earl, "Impact of lightning diverter strips on antenna radiation patterns," in *2020 14th European Conference on Antennas and Propagation (EuCAP)*, 1–5, Copenhagen, Denmark, Mar. 2020.

[19] Zheng, Y., A. Vukovic, P. Sewell, and A. Hall, "EM performance of segmented diverter strips used in lightning protection of wind turbine blades," in *2021 Asia-Pacific International Symposium on Electromagnetic Compatibility (APEMC)*, 1–4, Nusa Dua - Bali, Indonesia, Sep. 2021.

[20] Chen, H., F. Wang, Z. He, Z. Yue, *et al.*, "Plasma discharge characteristics of segmented diverter strips subject to lightning strike," *Plasma Science and Technology*, Vol. 21, No. 2, 025301, 2018.

[21] Ulmann, A., P. Brechet, A. Bondiou-Clergerie, A. Delannoy, P. Lalande, P. Blanchet, P. Laroche, E. Bocherens, G. L. Bacchiega, and I. Gallimberti, "New investigations of the mechanisms of lightning strike to radomes Part I: Experimental study in high voltage laboratory," *SAE Transactions*, 325–331, 2001.

[22] Karch, C., C. Paul, and F. Heidler, "Lightning strike protection of radomes," in *2019 International Symposium on Electromagnetic Compatibility — EMC EUROPE*, 650–655, Barcelona, Spain, Sep. 2019.

[23] Karch, C., W. Wulbrand, H. W. Zaglauer, and C. J. Hardwick, "An approach to determining radome diverter strip geometry," *Proceedings of the ICOLSE*, 16–19, 2003.

[24] Chen, C., W. Yan, Y. Zhao, E. Wang, C. Fu, R. Ma, and J. Zhu, "Simulation and analysis of EMP transient electromagnetic effect of aircraft," *The Journal of Engineering*, Vol. 2019, No. 16, 2464–2467, 2019.

[25] Vukovic, A., P. Sewell, and T. M. Benson, "Generating radome geometries for full lightning protection studies," in *2019 ESA Workshop on Aerospace EMC (Aerospace EMC)*, 1–5, IEEE, 2019.

[26] Fisher, F. A. and J. A. Plumer, "Lightning protection of aircraft handbook," Tech. Rep., Repository & Open Science Acess Portal (ROSA P), 2022.

[27] Goodloe, C., "Lightning protection guidelines for aerospace vehicles," Tech. Rep., Marshall Space Flight Center, NASA, 1999.

[28] Karch, C., W. Lick, and S. Pack, "Full-scale high voltage radome initial leader attachment tests," in *International Conference on Lightning and Static Electricity: Wichita, KS, USA*, 2019.

[29] Padoan, F., D. Clark, A. Haddad, C. Karch, and P. Westphal, "Initiation of electrical discharge at the triple junction of the lightning protection of an aircraft radome," *IEEE Electrical Insulation Magazine*, Vol. 39, No. 1, 6–16, 2022.

[30] Systèmes,Dassault, "CST Studio Suite — Electromagnetic Field Simulation Software," Dassault Systèmes, Germany, [Online]. Available: https://www.3ds.com/products/simulia/cst-studio-suite, 2024.

[31] Karch, C., M. Calomfirescu, M. Rothenhäusler, C. Brand, and H. Meister, "FFS: Lightning strike protection of radomes — An overview," Deutsche Gesellschaft für Luft-und Raumfahrt-Lilienthal-Oberth eV, 2017.

[32] Plumer, J. A. and L. C. Hoots, "Lightning protection with segmented diverters," in *1978 IEEE International Symposium on Electromagnetic Compatibility*, 1–8, IEEE, 1978.